Historical Biology

An International Journal of Paleobiology

ISSN: (Print) (Online) Journal homepage: https://www.tandfonline.com/loi/ghbi20

Pathological ribs in sauropod dinosaurs from the Middle Jurassic of Yunyang, Chongqing, Southwestern China

Chao Tan, Hai-Dong Yu, Xin-Xin Ren, Hui Dai, Qing-Yu Ma, Can Xiong, Zhi-Qiang Zhao & Hai-Lu You

To cite this article: Chao Tan, Hai-Dong Yu, Xin-Xin Ren, Hui Dai, Qing-Yu Ma, Can Xiong, Zhi-Qiang Zhao & Hai-Lu You (2022): Pathological ribs in sauropod dinosaurs from the Middle Jurassic of Yunyang, Chongqing, Southwestern China, Historical Biology, DOI: 10.1080/08912963.2022.2045979

To link to this article: https://doi.org/10.1080/08912963.2022.2045979

Published online: 28 Feb 2022.

HISTORICAL BIOLOGY
https://doi.org/10.1080/08912963.2022.2045979

Taylor & Francis
Taylor & Francis Group

Pathological ribs in sauropod dinosaurs from the Middle Jurassic of Yunyang, Chongqing, Southwestern China

Chao Tan[a,b,c], Hai-Dong Yu[b,c], Xin-Xin Ren[d], Hui Dai[b,c], Qing-Yu Ma[b,c], Can Xiong[b,c], Zhi-Qiang Zhao[e,f] and Hai-Lu You[g,h,i]

[a]Institute of Sedimentary Geology, Chengdu University of Technology, Chengdu, Sichuan, P. R. China; [b]No. 208 Hydrogeological and Engineering Geological Team, Chongqing Bureau of Geological and Mineral Resource Exploration and Development, Chongqing, P. R. China; [c]Chongqing Key Laboratory of Paleontology and Paleoenvironment Co-evolution (Sichuan-chongqing Joint Construction), Chongqing, P. R. China; [d]Institute of Geology, Chinese Academy of Geological Sciences, Beijing, P. R. China; [e]Zigong First People's Hospital, Zigong, Sichuan, China; [f]e GE China Innovation Center, General Electric Company, Chengdu, Sichuan, China; [g]Key Laboratory of Vertebrate Evolution and Human Origins of Chinese Academy of Sciences, Institute of Vertebrate Paleontology and Paleoanthropology, Chinese Academy of Sciences, Beijing, P. R. China; [h]CAS Center for Excellence in Life and Paleoenvironment, Beijing, P. R. China; [i]College of Earth and Planetary Sciences, University of Chinese Academy of Sciences, Beijing, P. R. China

ABSTRACT

Palaeopathological analyses have great potential to provide insights into dinosaurs' palaeobiology and life histories, but few cases have been reported in China. In this study, we report on four pathological sauropod ribs excavated in the same quarry of the Middle Jurassic in Yunyang County, Chongqing, southwest China. Based on morphological observation, computerised tomography (CT)-based energy spectrum data, and image analyses, three types of pathology were identified: traumatic fracture, fracture after bone infection, and osteosclerosis. This study increases the knowledge of dinosaur pathology, especially of Jurassic sauropods, and highlights the use of energy spectrum CT in palaeopathological studies.

ARTICLE HISTORY
Received 8 January 2022
Accepted 21 February 2022

KEYWORDS
Sauropod; rib; pathology; CT scan; Yunyang

Introduction

Palaeopathology focuses on ancient diseases and traumatic injuries in fossilised records (Tanke and Rothschild 2002) that allow unique insights into the palaeobiology and life histories of extinct animals (e.g., Rothschild and Diedrich 2012; Gonzalez et al. 2017). Palaeopathology has made great progress in recent decades, including more fossil records reported as well as a great development in technological methods. Osseous pathological records have been well documented in both ornithischian and saurischian dinosaurs, including reports on ornithischians (e.g., Witzmann et al. 2008; Tanke and Rothschild 2010; Hao et al. 2018); sauropodomorphs (e.g., Rothschild and Molnar 2005; Butler et al. 2013; Martinelli et al. 2014; Gonzalez et al. 2017; Barbosa et al. 2018); and theropods (e.g., McWhinney et al. 2001; Molnar 2001; Hanna 2002; Rothschild; Xing et al. 2018;; Farke and O'Connor 2007; Xing et al. 2009). According to recent records, almost all portions of the body (including the crania, vertebrae, girdles and limbs) could have pathological disease (Hanna 2002; Xing et al. 2009; Redelstorff et al. 2015; Dumbravă et al. 2016; Barbosa et al. 2018; Hunt et al. 2019; Cruzado-Caballero et al. 2021). To date, only five dinosaur pathological cases have been reported from China, namely, caudal vertebra of *Lufengosaurus huenei* (Xing et al. 2015, ZLJT001), ribs of *Lufengosaurus huenei* (Xing et al. 2018, YX V0003), femur of Gigantspinosaurus sichuanensis (Hao et al. 2018, 2020, ZDM0019), scapula of Yangchuanosaurus hepingensis (Xing et al. 2009, ZDM0024) and the fibula of psittacosaurids (Lü et al. 2007, JZMP-V-11).

Six palaeopathological types have been identified in prior research, namely, fractures, infections, osteopetrosis, degenerative disorders, tumours and developmental disorders (Witzmann et al. 2008; Chinsamy and Tumarkin-Deratzian 2009; Tanke and Rothschild 2014; Anné et al. 2016; de Souza Barbosa et al. 2016; Hao et al. 2020). Although many cases have been reported, many have not been well analysed due to methodological limitations. Recently, a new dinosaur fauna was discovered in Yunyang, Chongqing, in southwest China (Tan et al. 2018, 2020). The fossils appear to be from the Middle Jurassic Shaximiao Formation and already reflect rich diversity (Dai et al. 2020; Tan et al. 2020; Li et al. 2021; Ma et al. 2021). In this study, we report the pathology of four ribs employing multiple method analyses (including morphological comparison, analyses of computerised tomography [CT]-based energy spectrum data and image analysis).

Materials and methods

Materials

Four pathological ribs, namely, (6414-S18(1), 6515-S13(34), 6515-S13(23) and 3705-S12(1), were excavated at the same bone-bearing quarry in Yunyang, Chongqing, southwest China. The horizon of these materials is from the Lower Shaximiao Formation (Bajocian-Bathonian) (Figure 1). The bones were isolated, probably from several individuals. Distinctly abnormal enlargement was found on the tubercle and shaft of these ribs. It was determined that these ribs belonged to sauropod individuals because of their sub-elliptical to elliptical-shaped cross-sections, which differ from the platy-shaped cross-section of theropod and ornithischian dinosaurs. The ribs are probably from *Omeisaurus* or *Shunosaurus*, which have been reported from this quarry (Tan et al. 2020; Ma et al. 2021).

Method

Besides general observations of morphological features, energy spectrum CT scanning, three-dimensional reconstruction and data analysis techniques were also employed on all of the ribs, focusing on the

CONTACT Hai-lu You youhailu@ivpp.ac.cn Key Laboratory of Vertebrate Evolution and Human Origins of Chinese Academy of Sciences, Institute of Vertebrate Paleontology and Paleoanthropology, Chinese Academy of Sciences, Beijing, P. R. China

Published online 28 Feb 2022

pathologic area. Energy spectrum CT uses two basic substances to draw the energy spectrum curve of the measured substance and then compare it with the curve of a known substance to determine composition. The ribs were scanned using a GE Revolution 256, an analytical tectonic CT scanner from the Department of Radiology, Zigong First People's Hospital, Sichuan Province, China. The ribs were scanned using an axis sweep, with 80–140 Kv switching, a bulb speed of 0.5 ms, current at 485 mA and a slice thickness of 1.25 mm. Analysis of the energy spectrum of the energy-based material and drawing of the energy spectrum of the relevant region were carried out. Conventional CT scans, energy spectrum CT scans, and 3D-imaging were employed on all of the ribs. The energy spectrum CT removes the hardened artefact interference of the 140 kVp mode of hybrid energy and uses instantaneous switching of high and low dual-energy (80 kVp and 140 kVp) in a single tube to generate fully matched dual-energy data.

Result

Morphological pathological features

Rib 6414-S18 (1) (Figure 2a): This rib is partly preserved. It is dorsoventrally extended with an elliptical cross-section in outline. The cross-section of the proximal portion is sub-circular; by contrast, the cross-section of the distal end is elliptical. Three prominent swollen calluses are observed on the shaft (Figure 2a: 1, 2, 3): the distance between 1 and 2 is 9 cm, and that between 2 and 3 is 5 cm. There is an obvious shift on 1, and no prominent shift exists for 2 and 3. The cross-section line of these calluses obliquely intersects with the cross-section of the shaft. Distinct dislocation exists on a portion of callus on the shaft. This phenomenon belongs to traumatic fractures (Qin 2004).

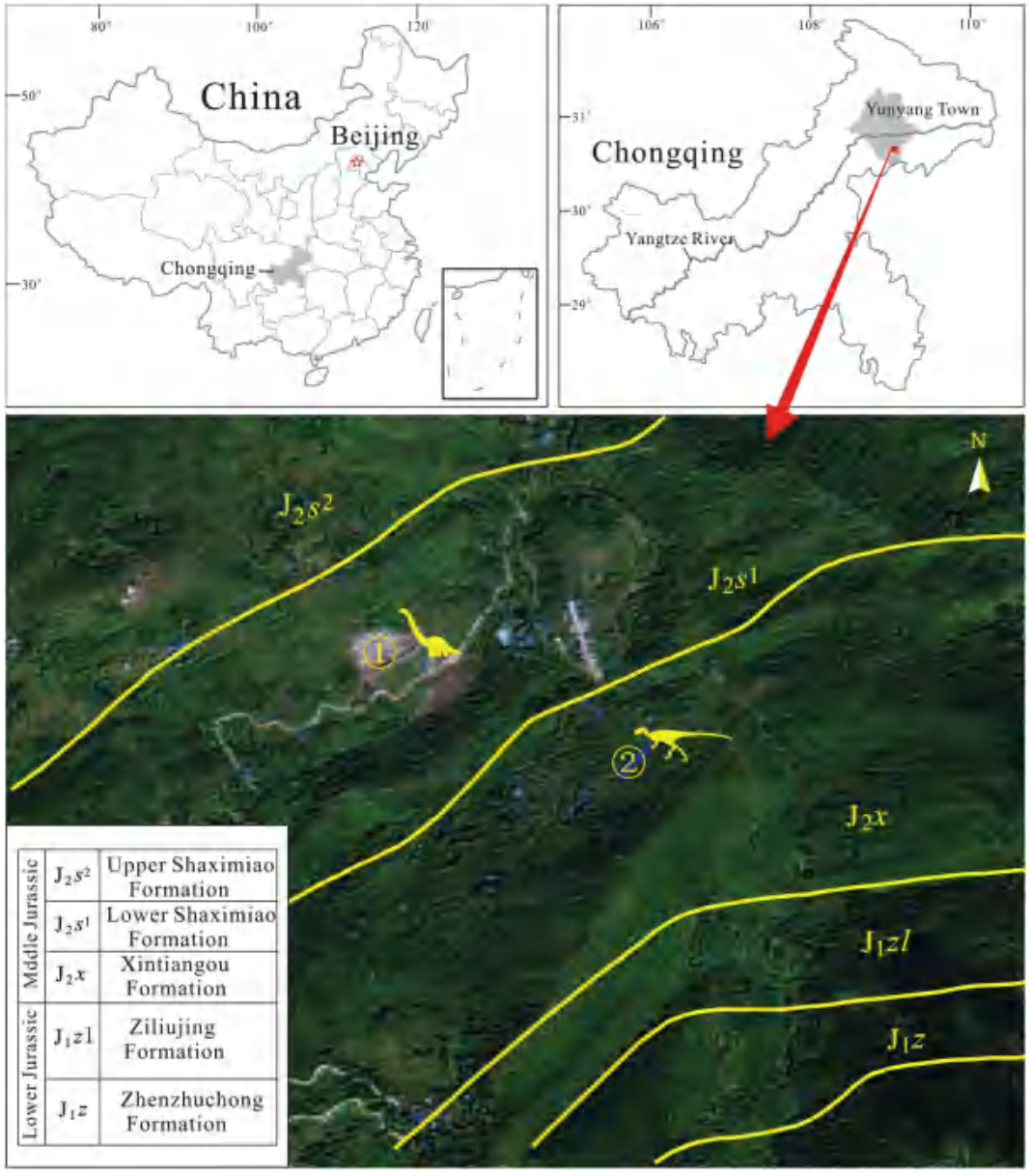

Figure 1. Geographic map showing dinosaur-bearing horizons. ①Omeisaurus puxiani and Shunosaurus lii in Lower Shaximiao Formation; ② Yunyangosaurus puanensis and Sanxiasaurus modaoxiensis in Xintiangou Formation.

Figure 2. Pathological sauropod ribs in this study. a: 6414-S18(1) and b 6515-S13(23) in four different views, respevtively. Scale bar equals 10 cm.

Rib 6515-S13(23): This dorsal rib is generally well preserved with the distal portion missing. In an anterior or posterior view, the capitulum is prominently medially extended compared with the tuberculum. The proximal portion of the shaft is abnormally enlarged (the perimeter of the enlargement is about 120 mm, and the perimeter of the shaft nearby is about 96 mm). The enlarged portion at the medial portion is much more prominent and extends about 4 cm along the shaft (Figure 2b).

Rib 6515-S13(34): This rib is partly preserved with a segmental shaft left. The middle portion of the preserved shaft is distinctly enlarged at the medial portion of the rib, and this enlargement extends about 6 cm along the shaft. The perimeter of the enlargement is about 120 mm, whereas the portion of the shaft nearby is about 100 mm. This further makes the proximal portion of the shaft irregularly curved (Figure 3a).

Rib 3705-S12(1) (Figure 3b): This dorsal rib is partially preserved, with the proximal portion well preserved. The capitulum articular is elliptical in outline. The diameter and perimeter of this articular are about 30 mm and 78 mm, respectively. In contrast, the sub-circular tuberculum is much larger than the capitulum, with a diameter and perimeter of 85 mm and 210 mm, respectively, or about five times the size of the capitulum in width. The articular surface of the tuberculum has no sign of anything unusual, but it is prominently expanding in almost all directions. The shaft is regular, the cross-section is plank-like and the anteroposterior breadth is more than three times the mediolateral breadth.

The shafts of 6515-S13(23) and 6515-S13(34) are irregularly enlarged. By contrast, the enlargement of the two ribs is much smaller than that of 3705-S12(1). The surfaces of the two shafts are smooth with no dislocation. Between 6515-S13(23) and 6515-S13(34), the abnormal enlargement on 6515-S13(23) expends in almost all directions, while the location of the enlargement on 6515-S13(34) seems particularly extended on the medial portion of the shaft.

CT image analysis

We employed the images of transverse, dorsal and mid-sagittal planes for the pathological analysis. The outline of each shaft is visible in the CT images. The degree of shading in the CT image represents the different bone densities and reflects different bone components. Cortical bone, the medullary cavity and the boundary between these two areas are prominent and easy to recognise (Fig. 4), especially in the pseudo-colour image (Fig. 4a_3,b_3,c_3,d_3). Areas on each element filled with greenish-black represent the glue filled in the fractures.

In the dorsal and transverse plane views, the widths of the medullary cavity are much larger than that of the cortical bone on rib 6414-S18(1), 6515-S13(23) and 6515-S13(34); this ratio is much bigger in 6515-S13(23) and 6515-S13(34). By contrast, this ratio on rib 3705S-S12(1) is in the opposite condition: the medullary cavity is notably compressed and shows a narrow curve in the CT image (Fig. 3b2). The boundary of the convex

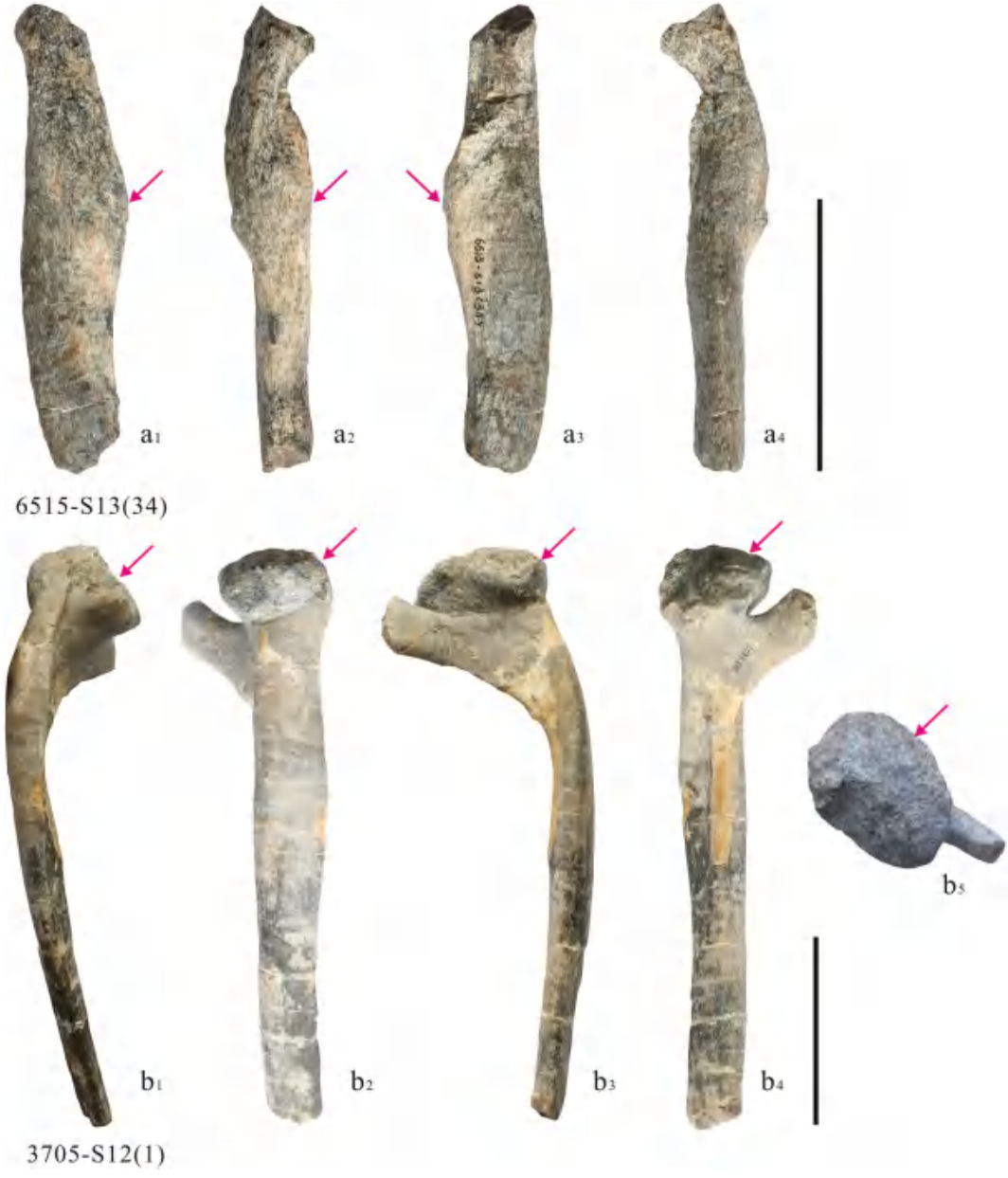

Figure 3. Pathological sauropod ribs in this study. a: 6515-S13(34) and b: 3705-S12(1) in four and five different views. Scale bar equals 10 cm.

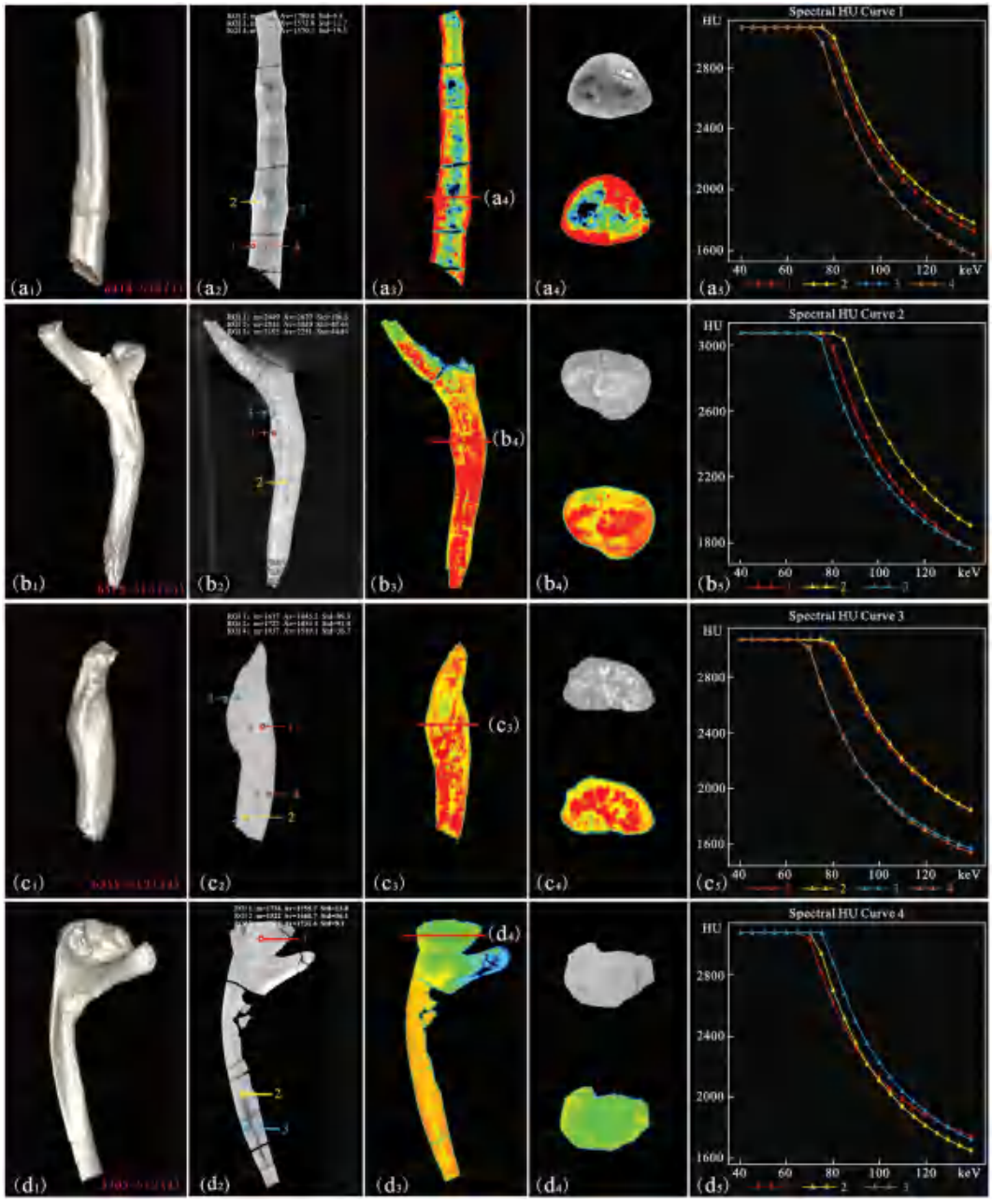

Figure 4. 3D and CT images for the pathological sauropods ribs in this study. a-d, 6414-S18(1), 3705-S12(1), 6515-S13(23), and 6515-S13(34) in 3D image (1), CT image with para-sagittal view (2), pseudo-color image with para-sagittal view (3), CT and Pseudo-color image with cross-section view (4), and energy spectrum image (5).

region reflects the boundary of the pathological area. Some oblique traces exist on the convexity of 6414-S18(1), and the extended directions are similar to the surrounding surfaces. Compared with the aforementioned materials, the width of the medullary cavity in 6515-S13(23) and 6515-S13(34) are distinctly decreased, with a distinct thicker cortical bone.

The segments of the cross-section reflect the irregular area. Some areas of rib 6414-S18(1) appear comparatively dense, and there are also areas from which the minerals seem to have partly dissolved to create an appearance of holes in the matrix; this is similar to the appearance of some fracture cases. The materials of rib 6515-S13 (23) and 6515-S13 (34) are not homogenous, which may result from some pathological influence. In 3705S-12 (1), areas of the bone appear uniformly dense and the medullary cavity is invisible.

Energy spectrum data analysis

Each substance has a specific attenuation coefficient, and the CT energy spectrum data can intuitively reflect substances' attenuation characteristics and can thus be used to distinguish different substance components. The value of m and Av represent the content of calcium hydroxyphosphate (HAP), the main element of each bone, in the target area, where 'm', 'Av' and 'Std' represent the minimum, average and standard deviation, respectively. The value of HAP in the cortical bone is normally greater than in the medullary cavity (Deng et al. 2010). The energy spectrum curve easily reflects the homology of matter, and this curve may reflect the prominent difference between the cortical bone and medullary cavity (Hao et al. 2018).

In the CT figure of Rib 6414-S18(1) (Fig. 4a$_1$), mark 2 and mark 3 represent the pathological area of the cortical bone and medullary cavity, respectively. By contrast, mark 1 and mark 4 represent normal bone features. The value of 'm' and 'Av' at mark 2 is much bigger than at marks 3 and 4, which indicates the HAP of the cortical bone is greater than the medullary cavity. In a normal situation, curves 1 and 2 should interlap with each other (like curves 3 and 4), whereas those show a similar spectrum curve (i.e., generally parallel on curve 1 and curve 2). No overlapped energy spectrum curves at 1 and 2 represent the abnormal areas that have not suffered pathological changes. Combing morphological and CT images analysis, non-superposition for curve 2 may cause calluses. Curves 3 and 4 represent the medullary cavity, and they indicate the abnormal and normal areas that share consistent homology. We suggest the cortical portion of the abnormal area healed during the plastic period with the medullary cavity connected.

In the CT image of Rib 6515-S13(23) (Fig. 4b$_2$), marks 1, 2 and 3 represent the abnormal area, medullary cavity and cortical bone, respectively. Energy spectrum curve 1 of the abnormal area is situated between curve 2 (medullary cavity) and 3 (cortical bone). It is worth noting that the value of HAP on mark 1 is between those of marks 2 and 3. This situation is generally opposite to the normal condition. The HAP values on all of the marks for 6515-S13(23) are greater than those for the other ribs; we suggest this condition may be caused by a pathological affection that makes the entire shaft abnormal.

Marks 1 to 4 in the CT image of 6515-S13(34) represents the cortical bone and medullary cavity on expanded and unexpanded areas, respective (Fig. 4c$_2$). Curves 1 and 2 and Curves 3 and 4 generally coincide in this image, which indicates that the component is consistent. The HAP values for 6515-S13(34) are similar to those for 6515-S13(23). Taking the same quarry in which the two elements were excavated into consideration, we speculate these are in the same individual and the lesions are due to some kind of disease.

Mark 1 on Rib 3705-S12(1) in the CT image (Fig. 4d$_2$) is a prominent abnormal area, while marks 2 and 3 represent the medullary cavity and cortical bone, respectively. The HAP values for marks 1 and 3 are much similar to mark 2. The position of mark 1 belongs to the medullary cavity, which indicates the components of the abnormal area are generally similar for the cortical bone and medullary cavity. On the energy spectrum image (Fig. 4b$_5$), the three curves follow completely different trends. Both the CT image and energy spectrum values reflect strong reconstruction in the medullary cavity. In human bone sclerosis, bone mineral density is strongly increased in the medullary portion compared with the generally normal value on the cortical portion, and we suggest bone sclerosis is similarly presenting in Rib 3705-S12(1).

Discussion

Many paleo-pathological cases on ribs reported in dinosaurs belong to theropods, stegosaurs, hadrosaurs and sauropodomorphs, and pathological types include fracture, infection, sclerosis and tumour (Hanna 2002; Straight et al. 2009; Bell 2010; Bell and Coria 2013; Xing et al. 2018; Hunt et al. 2019). The presence of fractures in dinosaurs tends to be more abundant in the axial skeleton and proximal areas of the body and pes (Sullivan et al. 2000; Hanna 2002; Rothschild and Martin 2006; Arbour and Currie 2011; Peterson and Vittore 2012; Hearn and Williams 2019; Cruzado-Caballero et al. 2021). Rothschild and Martin (2006) divided fractures into seven types depending on mechanical principles: oblique (which can be closed or displaced), transverse, greenstick, spiral, compression, impact and stress. Fractures can be classified as traumatic or atraumatic, while Hao et al. (2020) employed medical research methods to divide fractures into traumatic and pathologic fractures. When a traumatic fracture is healed, it not only shows a wide range of bone bruises but also oblique creases (Rothschild and Martin 1993, 2006; Lovell 1997; Qin 2004; Cruzado-Caballero et al. 2021).

Infection can also appear during the lifetime (Hunt et al. 2019), and osteomyelitis is also a type of infection (Miller 2008). Fractures include infectious (resulting from infection of osteomyelitis) and traumatic-infectious (injury followed by secondary infection) (Bell and Coria 2013). An infectious abscess is a signal for the presence of reactive new lamellar bone, which appears in response to infection with a narrow zone of transition, lytic, geographic lesion characteristics (Rothschild et al. 1999; Rothschild and Martin 2006). Sclerosis is rare in fossil cases, and in dinosaurs, the femur of *Mussaurus patagonicus* (Dinosauria: Sauropodomorpha) shares these features (Cerda et al. 2014). These cases of sclerosis show compaction of the medullary region, an unevenly developed cortical region and significant densification. This is related to a failure of resorption of the bone deposited on the calcified cartilage of growth centre, or failure to produce a normal marrow cavity in long bones (Tolar et al. 2004; Stark and Savarirayan 2009).

Three bone calluses and oblique creases appear prominently on rib 6414-S18(1), although osteomalacia could cause bone deformation and more prominent decreased bone density and blurred cortical margins. The callus on rib 6414-S18(1) shares prominent displacement, and the CT and energy spectrum images show the bone cortex was in the period of shaping. The medullary cavity is connected, and we suggest this belongs to a traumatic fracture, in the late stages of fracture healing. The direction of the oblique creases reflects the force direction of the trauma, and the maximum displacement of the bone represents the primary force-bearing point. Three or more broken marks (the callus portions) on the same rib indicate the trauma was severe, with comminuted fractures.

Rib 6515-S13(34) and 6515-S13(23) share a similar situation: expanded but no oblique crease on the shafts; the cortical bone invades into the medullary cavity on the pathological area; composed substances on the medullary cavity are not different in the CT images, whereas lytic lesions appear in the cortical region; and the HAP content of the medullary cavity is much higher than that in the cortical bone. There are also some differences in these elements. Like the two aforementioned elements (6515-S13(34) and 6515-S13 (23)), the shaft of 6515-S13(23) is prominently expanded; by contrast, that swollen shaft seems directional and the cortical bone is distinctly enlarged on 6515-S13(34). Considering these two elements were excavated in the same quarry, we infer these could be from one individual. In records of living animals and human beings, a simple infection does not usually cause bone (non-joint) enlargement. A single stress fracture could only lead to bone formation, other than the medullary or cortical confusion (e.g. rib 6414-S18(10)). By contrast, infection and tumour could inevitably cause changes in the medullary cavity and cortex. In short, we suggest these two ribs suffered infection, and the infection caused osteomyelitis. The infection then spread throughout the whole shaft, and minor external trauma occurred. This condition is significantly weaker than *Gigantspinosaurus sichuanensis* (see Hao et al. 2018). Infection places high physiological demands on an individual, requiring strong immune and inflammatory responses (Gross et al. 1993). Trauma could lead to infection, which could extend to the whole body, and infection is then in turn more susceptible to trauma. Thus, infection and trauma are inseparable.

The articular surface of rib 3705-S12(1) is prominently extended, and the medullary cavity is strongly transformed. The cortical and cancellous bone regions are significantly increased on the whole rib, similar to the features of osteopetrosis (Brothwell 2002). This condition is distinctly different from rib 6515-S13(23), and some classic osteomyelitis cases (García et al. 2017). Arthritis usually begins with soft tissue swelling and osteoporosis, and later with the destruction of weight-bearing bone. Bone enlargement of rib 3705-S12(1) appears on this scale, with the enlargement on the articular portion of the capitulum, and the disease appears to have affected the entire shaft. We therefore suggest the aetiology of these materials is complex, and osteopetrosis caused abnormal extension on the rib (3705-S12(1)).

Palaeopathological analysis of numerous dinosaur bone samples may shed light on dinosaur behaviour, environmental influences and physiology (Hanna 2002). Lesions on or injuries to the ribs would not directly affect the mobility as would damage to the limbs or vertebrae on dinosaurs, whereas, regardless of the type of pathology, a local sign of inflammation and pain might have yielded clinical features presented by the individual. By contrast, a healed fracture would not directly kill a dinosaur, but may cause a decline in the immune system, leading to the occurrence of other lesions. Osteosclerosis on the capitulum could even produce spinal ligament ossification. Fewer cases have been reported in herbivorous dinosaurs than in carnivorous dinosaurs, because herbivorous dinosaurs are more likely to die of predation (Rothschild 1988), while carnivorous dinosaurs are more likely to become injured than herbivorous dinosaurs (Molnar and Farlow 1990; Hanna 2002). This study adds four more herbivorous cases.

Conclusions

This study identified three types of pathology ribs in four ribs. The callus and oblique fracture on rib 6414-S18(1) reflects a traumatic fracture; ribs 6515-S13(34) and 6515-S13(23) belong to a case of pathologic fracture with the union after bone infection. Rib 3705-S12(1) is prominently expanding and constitutes a case of osteosclerosis. We suggest energy spectrum CT scanning is a significant tool for better identifying pathological types, as it allows us to observe internal density, matrix content and cortical and medullary differentiation without destroying the materials. These abnormal materials from the same quarry may indicate a notable number of individuals with diseases in the fauna. This study enriches the further understanding of dinosaur fauna in the Middle Jurassic.

Acknowledgments

For their hospitality, we wish to thank Zhang Yu-Qing for the dinosaur material reparation, Li Qi for taking photographs of the specimens and Feng Hao from No. 1 People's Hospital of Zigong for taking a CT scan of the specimens. We are grateful to Peng Guang-Zhao, Ye Yong, Jiang Shan and Hao Bao-Qiao for their helpful discussion. Thoughtful reviewers and the editor improved an earlier version of this manuscript.

Disclosure statement

No potential conflict of interest was reported by the author(s).

Funding

This work was supported by the the Strategic Priority Research Program of the Chinese Academy of Sciences [XDB26000000]; National Natural Science Foundation of China [41688103, 41872021, 42102018].

ORCID

Hai-Lu You http://orcid.org/0000-0003-2203-6461

References

Anné J, Hedrick BP, Schein JP. 2016. First diagnosis of septic arthritis in a dinosaur. R Soc Open Sci. 3:160222. doi:10.1098/rsos.160222.

Arbour VM, Currie PJ. 2011. Tail and pelvis pathologies of ankylosaurian dinosaurs. Hist Biol. 23(4):375–390. doi:10.1080/08912963.2011.563849.

Barbosa FHS, Ribeiro IC, Pereira PVLGC, Bergqvist LP. 2018. Vertebral lesions in a titanosaurian dinosaur from the Early-Late Cretaceous of Brazil. Geobios. 51:385–389. doi:10.1016/j.geobios.2018.08.002.

Bell PR. 2010. Palaeopathological changes in a population of Albertosaurus sarcophagus from the Upper Cretaceous Horseshoe Canyon Formation of Alberta, Canada. Can J Earth Sci. 47(9):1263–1268. doi:10.1139/E10-030.

Bell PR, Coria RA. 2013. Palaeopathological survey of a population of Mapusaurus (Theropoda: Carcharodontosauridae) from the Late Cretaceous Huincul Formation, Argentina. PloS one. 8(5):e63409. doi:10.1371/journal.pone.0063409.

Brothwell D. 2002. Ancient avian osteopetrosis: the current state of knowledge. In: Proceedings of the 4th Meeting of the ICAZ Bird Working Group Kraków, Poland. Acta Zool Cracoviensia. 45:315–318.

Butler RJ, Yates AM, Rauhut OWM, Foth C. 2013. A pathological tail in a basal sauropodomorph dinosaur from South Africa: evidence of traumatic amputation? J Vertebr Paleontol. 33:224–228. doi:10.1080/02724634.2012.710691.

Cerda IA, Chinsamy A, Pol D. 2014. Unusual endosteally formed bone tissue in a Patagonian basal sauropodomorph dinosaur. Anat Rec. 297(8):1385–1391. doi:10.1002/ar.22954.

Chinsamy A, Tumarkin-Deratzian A. 2009. Pathologic bone tissues in a Turkey vulture and a nonavian dinosaur: implications for interpreting endosteal bone and radial fibrolamellar bone in fossil dinosaurs. Anat Rec. 292:1478–1484. doi:10.1002/ar.20991.

Cruzado-Caballero P, Díaz-Martínez I, Rothschild B, Bedell M, Pereda-Suberbiola X. 2021. A limping dinosaur in the Late Jurassic: pathologies in the pes of the neornithischian Othnielosaurus consors from the Morrison Formation (Upper Jurassic, USA). Hist Biol. 33(9):1753–1759. doi:10.1080/08912963.2020.1734589.

Dai H, Ma Q, Hu X, Zhou Y, Tan C, Li N. 2020. A new dinosaur Fauna is discovered in Yunyang, Chongqing, China. Acta Geol Sin (English Edition). 94(1):216. doi:10.1111/1755-6724.14516.

de Souza Barbosa FH, da Costa PVLG, Bergqvist LP, Rothschild BM. 2016. Multiple neoplasms in a single sauropod dinosaur from the Upper Cretaceous of Brazil. Cretaceous Res. 62:13–17. doi:10.1016/j.cretres.2016.01.010.

Deng JG, Peng GZ, Jin YZ, Ye Y. 2010. Study on the characterization of dinosaur fossils and their surrounding rocks from Zigong. Chin J Spectrosc Lab. 1:192–196.

Dumbravă MD, Rothschild BM, Weishampel DB, Csiki-Sava Z, Andrei RA, Acheson KA, Codrea VA. 2016. A dinosaurian facial deformity and the first occurrence of ameloblastoma in the fossil record[J]. Sci Rep. 6(1):1–7. doi:10.1038/srep29271.

Farke AA, O'Connor PM. 2007. Pathology in Majungatholus crenatissimus (Theropoda, Abelisauridae) from the Late Cretaceous of Madagascar. Memoir Soc Verteb Paleontol. 8:180–184. doi:10.1671/0272-4634(2007)27[180:PIMCTA]2.0.CO;2.

García RA, Cerda IA, Heller M, Rothschild BM, Zurriaguz V. 2017. The first evidence of osteomyelitis in a sauropod dinosaur. Lethaia. 50(2):227–236. doi:10.1111/let.12189.

Gonzalez R, Gallina PA, Cerda IA. 2017. Multiple paleopathologies in the dinosaur Bonitasaura salgadoi (Sauropoda: Titanosauria) from the Upper Cretaceous of Patagonia, Argentina. Cretaceous Res. 79:159–170. doi:10.1016/j.cretres.2017.07.013.

Gross J, Rich T, Vickers–Rich P. 1993. Dinosaur bone infection. Res Explor. 9:286–293.

Hanna RR. 2002. Multiple injury and infection in a sub-adult theropod dinosaur Allosaurus fragilis with comparisons to allosaur pathology in the cleveland-lloyd dinosaur quarry collection. J Vertebr Paleontol. 22:76–90. doi:10.1671/0272-4634(2002)022[0076:MIAIIA]2.0.CO;2.

Hao BQ, Feng H, Zhao ZQ, Ye Y, Wan DX, Peng GZ. 2020. Different types of bone fractures in dinosaur fossils. Hist Biol. doi:10.1080/08912963.2020.1722661.

Hao BQ, Ye Y, Maidment SCR, Bertazzo S, Peng GZ, and You HL. 2018. Femoral osteopathy in gigantspinosaurussichuanensis (Dinosauria: Stegosauria) from the Late Jurassic of Sichuan Basin, Southwestern China. Hist Biol. 32(8):1028–1035. doi:10.1080/08912963.2018.1561673.

Hearn L, Williams ACC. 2019. Pain in dinosaurs: what is the evidence? Philos Trans R Soc B. 374(1785):20190370. doi:10.1098/rstb.2019.0370.
Hunt TC, Peterson JE, Frederickson JA, Cohen JE, Berry JL. 2019. First documented pathologies in Tenontosaurus tilletti with comments on infection in non-avian dinosaurs. Sci Rep. 9(1):1–8. doi:10.1038/s41598-019-45101-6.
Li N, Dai H, Tan C, Hu X, Wei Z, Lin Y, Wei G, Li D, Meng L, Hao B, et al. 2021. A neornithischian dinosaur from the Middle Jurassic Xintiangou Formation of Yunyang, Chongqing, China: the earliest record in Asia. Hist Biol. 33 (7):1089–1102. doi:10.1080/08912963.2019.1679129.
Lovell NC. 1997. Trauma analysis in paleopathology. Am J Phys Anthropol. 104 (25):139–170.
Lü JC, Kobayashi Y, Lee YN, Ji Q. 2007. A new Psittacosaurus (Dinosauria: Ceratopsia) specimen from the Yixian Formation of western Liaoning, China: te frst pathological psittacosaurid. Cretaceous Res. 28:272–276. doi:10.1016/j.cretres.2006.08.005.
Ma QY, Dai H, Tan C, Li N, Wang P, Ren XX, Meng L, Zhao Q, Wei GB, Xu X. 2021. New Shunosaurus (Dinosauria: Sauropoda) material from the middle Jurassic lower Shaximiao Formation of Yunyang, Chongqing, China. Hist Biol. 1–15. doi:10.1080/08912963.2021.1962852.
Martinelli AG, Teixeira VPA, Marinho TS, Fonseca PHM, Cavellani CL, Araujo AJG, Ribeiro LCB, Ferraz MLF. 2014. Fused mid-caudal vertebrae in the titanosaur Uberabatitan ribeiroi from the Late Cretaceous of Brazil and other bone lesions. Lethaia. doi:10.1111/let.12117.
McWhinney L, Carpenter K, Rothschild B. 2001. Dinosaurian humeral periostitis: a case of a juxtacortical lesion in the fossil record. In: Tanke DH, Carpenter K, editors. Mesozoic Vertebrate Life. Bloomington: Indiana University Press; p. 364–377.
Miller TT. 2008. Bone tumors and tumorlike conditions: analysis with conventional radiography. Radiology. 246(3):662–674. doi:10.1148/radiol.2463061038.
Molnar RE. 2001. Theropod paleopathology: a literature survey. In: Tanke DH, Carpenter K, editors. Mesozoic Vertebrate Life. Bloomington: Indiana University Press; p. 337–363.
Molnar RE, Farlow JO. 1990. Carnosaur paleobiology. In: Weishampel DB, Dodson P, Osmolska H, editors. The Dinosauria. Berkeley: University of California Press; p. 210–224.
Peterson JE, Vittore CP. 2012. Cranial pathologies in a specimen of Pachycephalosaurus. PloS one. 7(4):e36227. doi:10.1371/journal.pone.0036227.
Qin Y. 2004. Fracture heeling, delayed union and nonunion. Chin J Orthop Trauma. 9:1059–1062.
Redelstorff R, Hayashi S, Rothschild BM, Chinsamy A. 2015. Non-traumatic bone infection in stegosaurs from Como Bluff, Wyoming. Lethaia. 48(1):47–55. doi:10.1111/let.12086.
Rothschild BM. 1988. Stress fracture in a ceratopsian phalanx. J Paleontol. 62:302–303. doi:10.1017/S0022336000029954.
Rothschild BM, Diedrich CJ. 2012. Pathologies in the extinct Pleistocene Eurasian steppe lion *Panthera leo* spelaea (Goldfuss, 1810) – results of fights with hyenas, bears and lions and other ecological stresses. Int J Paleopathol. 2:187–198. doi:10.1016/j.ijpp.2012.09.004.
Rothschild BM, Martin LD. 1993. Paleopathology: disease in the fossil record. Boca Raton: CRC Press; p. 386.
Rothschild BM, Martin LD. 2006. Skeletal impact of disease. Bull N Mex Mus Nat Hist Sci. 33:1–230.
Rothschild BM, and Molnar RE. 2005. Sauropod stress fractures as clues to activity. In: Tidwell V, and Carpenter K, editors. Thunder-lizards: the sauropodomorph di-nosaurs. Bloominston and Indianapolis: Indiana University Press; p. 381–392.
Rothschild BM, Witzke BJ, Hershkovitz I. 1999. Metastatic cancer in the Jurassic. Lancet. 354(9176):398. doi:10.1016/S0140-6736(99)01019-3.
Stark Z, Savarirayan R. 2009. Osteopetrosis. Orphanet J Rare Dis. 4(1):1–12. doi:10.1186/1750-1172-4-5.
Straight WH, Davis GL, Skinner HCW, Haims A, McClennan BL, Tanke DH. 2009. Bone lesions in hadrosaurs: computed Tomographic Imaging as a guide for paleohistologic and stable-isotopic analysis[J]. J Vertebr Paleontol. 29 (2):315–325. doi:10.1671/039.029.0211.
Sullivan RM, Tanke DH, Rothschild BM. 2000. An impact fracture in an ornithomimid (Ornithomimosauria: Dinosauria) metatarsal from the Upper Cretaceous (Late Campanian) of New Mexico. Bull N Mex Mus Nat Hist Sci. 17:109–111.
Tan C, Dai H, He JJ, Zhang G, Hu XF, Yu HD, Li N, Wei GB, Peng GZ, Ye Y, et al. 2018. Discovery of Omeisaurus (Dinosauria: Sauropoda) in the Middle Jurassic Shaximiao Formation of Yunyang, Chongqing, China. Verteb Palasiatica. doi:10.19615/j.cnki.1000-3118.181115.
Tan C, Xiao M, Dai H, Hu XF, Li N, Ma QY, Wei ZY, Yu HD, Xiong C, Peng GZ, et al. 2020. A new species of Omeisaurus (Dinosauria: Sauropoda) from the Middle Jurassic of Yunyang, Chongqing, China. Hist Biol. 1–13. doi:10.1080/08912963.2020.1743286.
Tanke DH, Rothschild BM. 2002. Dinosaurs: an annotated bibliography of dinosaur paleopathology and related topics 1838–2001. Bull N Mex Mus Nat Hist Sci. 20:1–97.
Tanke DH, Rothschild BM. 2010. Paleopathologies in Albertan ceratopsids and their behavioral significance. In: Ryan MJ, Chinnery-Allgeier BJ, Eberth DA, editors. New perspectives on horned dinosaurs. Bloomington and Indianapolis: Indiana University Press; p. 355–384.
Tanke DH, Rothschild BM. 2014. Paleopathology in Late Cretaceous Hadrosauridae from Alberta, Canada. In: Eberth DA, Evans DC, editors. Hadrosaurs. Bloomington: Indiana University Press; p. 540–571.
Tolar J, Teitelbaum SL, Orchard PJ. 2004. Osteopetrosis. N Engl J Med. 351 (27):2839–2849. doi:10.1056/NEJMra040952.
Witzmann F, Asbach P, Remes K, Hampe O, Hilger A, Paulke A. 2008. Vertebral pathology in an ornithopod dinosaur: a hemivertebra in Dysalotosaurus lettowvorbecki from the Jurassic of Tanzania. Anat Rec. 291:1149–1155. doi:10.1002/ar.20734.
Xing LD, Dong H, Peng GZ, Shu CK, Hu XD, Jiang H. 2009. A scapular fracture in Yangchuanosaurus hepingensis (Dinosauria, Theropoda). Geol Bull China. 28:1390–1395.
Xing L, Rothschild BM, Ran H, Miyashita T, Scott Persons W, IV, Sekiya T, Zhang J, Wang T, and Dong Z. 2015. Vertebral fusion in two Early Jurassic sauropodomorph dinosaurs from the Lufeng Formation of Yunnan, China. Acta Palaeontol Pol. 60(3):643–649.
Xing L, Rothschild BM, Randolph-Quinney PS, Wang Y, Parkinson AH, Ran H. 2018. Possible bite-induced abscess and osteomyelitis in Lufengosaurus (Dinosauria: sauropodomorph) from the Lower Jurassic of the Yimen Basin, China. Sci Rep. 8(1):1–8. doi:10.1038/s41598-018-23451-x.